#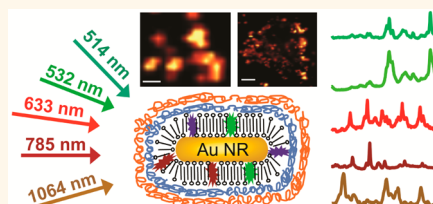 Universal Surface-Enhanced Raman Tags: Individual Nanorods for Measurements from the Visible to the Infrared (514−1064 nm)

Alison McLintock,[†,∥] Carlota A. Cunha-Matos,[‡,∥] Michele Zagnoni,[§] Owain R. Millington,[⊥] and Alastair W. Wark[†,*]

[†]Centre for Molecular Nanometrology, WestCHEM, Department of Pure and Applied Chemistry, University of Strathclyde, 295 Cathedral Street, Glasgow, U.K., G1 1XL, [‡]Department of Biomedical Engineering, University of Strathclyde, 106 Rottenrow, Glasgow, U.K., G4 0NW, [§]Centre for Microsystems and Photonics, Electronic and Electrical Engineering, University of Strathclyde, 204 George Street, Glasgow, U.K., G1 1XW, and [⊥]Centre for Biophotonics, Strathclyde Institute for Pharmacy and Biomedical Sciences, University of Strathclyde, 161 Cathedral Street, Glasgow, U.K., G4 0RE. [∥]A. McLintock and C. A. Cunha-Matos contributed equally.

ABSTRACT Surface-enhanced Raman scattering (SERS) is a promising imaging modality for use in a variety of multiplexed tracking and sensing applications in biological environments. However, the uniform production of SERS nanoparticle tags with high yield and brightness still remains a significant challenge. Here, we describe an approach based on the controlled coadsorption of multiple dye species onto gold nanorods to create tags that can be detected across a much wider range of excitation wavelengths (514−1064 nm) compared to

conventional approaches that typically focus on a single wavelength. This was achieved without the added complexity of nanoparticle aggregation or growing surrounding metallic shells to further enhance the surface-enhanced resonance Raman scattering (SERRS) signal. Correlated Raman and scanning electron microscopy mapping measurements of individual tags were used to clearly demonstrate that strong and reproducible SERRS signals at high particle yields (>92%) were readily achievable. The polyelectrolyte-wrapped nanorod−dye conjugates were also found to be highly stable as well as noncytotoxic. To demonstrate the use of these universal tags for the multimodal optical imaging of biological specimens, confocal Raman and fluorescence maps of stained immune cells following nanoparticle uptake were acquired at several excitation wavelengths and compared with dark-field images. The ability to colocalize and track individual optically encoded nanoparticles across a wide range of wavelengths simultaneously will enable the use of SERS alongside other imaging techniques for the real-time monitoring of cell−nanoparticle interactions.

KEYWORDS: surface-enhanced Raman · gold nanorod · single nanoparticle imaging and spectroscopy · cell imaging

Combining metallic nanoparticles and adsorbed reporter molecules to create substrates capable of producing bright surface-enhanced Raman scattering (SERS) signals has been an area of tremendous interest for a wide range of molecular sensing and labeling applications in recent years.[1] The attraction of SERS tags compared to fluorescent organic dyes and quantum dots for biological labeling is the potential for enhanced detection sensitivity and photostability along with the narrow line widths of vibrational bands allowing greater multiplexing capability. Also, by introducing organic reporter dyes whose absorption properties overlap with the local surface plasmon resonance (LSPR) of the nanostructure and the excitation laser

wavelength enables even greater signal enhancement *via* surface-enhanced resonance Raman scattering (SERRS).[2] However, despite these advantages, a number of limitations have restricted the successful development and application of Raman tags compared to fluorescent labeling.

The vast majority of SERS studies to date have focused on creating controlled aggregates of nanoparticles and placing reporter molecules in the vicinity of interparticle gaps. For quasi-spherical particles, the Raman enhancement of isolated particles is weak, and dramatic increases in signal are associated with interparticle plasmonic field coupling and the creation of "hot spots".[3] Several routes have been demonstrated for the preparation of small clusters of nanoparticles

and reporters that can then be encased in a protecting shell such as silica[4] or a polymer.[5] However, obtaining high yields of uniformly bright SERS active clusters within colloidal suspensions has proved difficult to fabricate, and the larger overall aggregate size may be impractical for many *in vivo* applications.

The creation of single nanoparticle SERS tags *via* simple design rules still remains a significant challenge.[6] The number of studies utilizing correlated Raman-structure measurements to investigate the SERS activity of individual nanoparticles[7−14] and aggregates[4,15−17] are still relatively few compared to bulk solution analyses. Recent efforts have focused on preparing anisotropic particle shapes featuring sharp edges that promote large electromagnetic fields. These include gold nanostars,[8] nanoshells,[9] spiked beads,[10] nanocubes,[11,18] octahedral structures[12] as well as roughened[13,14] particles up to several hundred nm in size. Enhanced signals can also be obtained when individual particles are in contact with a metallic layer[8,18,19] or assembled around a larger particle substrate.[20] Osberg *et al.* recently reported a SERS investigation of individual rod dimer structures created by lithography;[21] however, an experimental study of SERS activity at isolated single metallic nanorods prepared by colloidal synthesis has not been previously described in the literature. Recent studies involving SERS measurements of gold nanorods and attached reporter molecules include bulk solution measurements of both nonaggregated[22,23] and self-assembled systems[5,24,25] and following cellular uptake.[26,27]

In addition to investigating signal enhancement factors most SERS tags are tailored to a specific excitation wavelength, which is constrained by both the LSPR of the nanoparticles and the electronic properties of the reporter molecule. Recently, Van Duyne *et al.* demonstrated for nanoantenna dimers and trimers the excitation of additional "dark" plasmon modes in aggregates results in large SERS enhancement factors at wavelengths far from the LSPR of the nanoantenna.[15] For individual particles where no hybridization of plasmon modes occurs,[28,29] the demonstration of an approach that enables an individual nanoparticle to exhibit SERS activity across a wide range of wavelengths has not yet been demonstrated.

In this article, we introduce the concept of a *universal* SERRS tag (UST) featuring individual, nonaggregated nanoparticle conjugates capable of enhanced Raman signals across a wide range of laser excitation wavelengths extending from 514 to 1064 nm. This is in contrast to the vast majority of the literature on SERS tags which typically involves the added complexity of a nanoparticle aggregation step and optimizes the signal for only a single laser wavelength. The UST's are created by the well-controlled coadsorption of different dyes onto a gold nanorod (NR) surface which are then polymer wrapped to create a very stable colloidal suspension. By performing a correlated optical and scanning electron microscope (SEM) study at the single nanoparticle level as well as bulk solution measurements, the very high tag synthesis yields and strong SERRS signals at different excitation wavelengths are clearly demonstrated. It is envisioned that these UST's will be valuable for applications where they can be visualized across a wide spectral range such as for multimodal biological optical imaging.[30,31] This is emphasized by also performing a toxicology study alongside confocal Raman and fluorescent mapping of multiply stained dendritic cells following UST incubation.

RESULTS AND DISCUSSION

Universal SERRS Tag design. To realize the aim of creating a single nanoparticle SERRS tag capable of generating strong Raman signals across a wide range of excitation wavelengths (from 514 to 1064 nm), the route used in Figure 1(a) was explored for the production of UST's. A 1 L stock solution of gold nanorods was first prepared with 46 and 11 nm average length and width respectively, (see Supporting Information Figure S1 for electron micrographs) which was then repeatedly washed and resuspended in 1 mM CTAB. We have recently demonstrated that relatively hydrophobic dye molecules are readily sequestered into the CTAB bilayer when introduced to an aqueous nanorod solution.[22] A key advantage here is that both the fractional surface coverage and molecular orientation of the adsorbed dye molecules can be controlled much more effectively than conventional electrostatic approaches for nanoparticle dye functionalization. The nanorod−dye conjugate is then stabilized by wrapping with a negatively charged poly(sodium 4-styrenesulfonate), PSS layer. The final UST's reported in this study were also wrapped with a second positively charged layer of poly(diallyldimethylammonium chloride), PDDAC, and have remained stable in suspension at room temperature for longer than 15 months with no change in their optical properties (data not shown).

In order to determine which combination of dyes were most suitable for use as universal SERRS tags, a range of nanorod conjugates were prepared featuring only one dye and their optical properties compared. A summary of the absorption properties of the various dyes investigated are shown in Figure 1(b). Each dye used is structurally similar, each having a quaternary ammonium group (see Figure S2, Supporting Information) and are also relatively hydrophobic; thus, we expected each dye to have comparable affinities for the surrounding CTAB bilayer. The UV−vis spectra show that the absorbance of the dyes selected for comparison cover a broad range of wavelengths leading to the possibility of utilizing combinations of dyes to create tags that are Raman active across the most
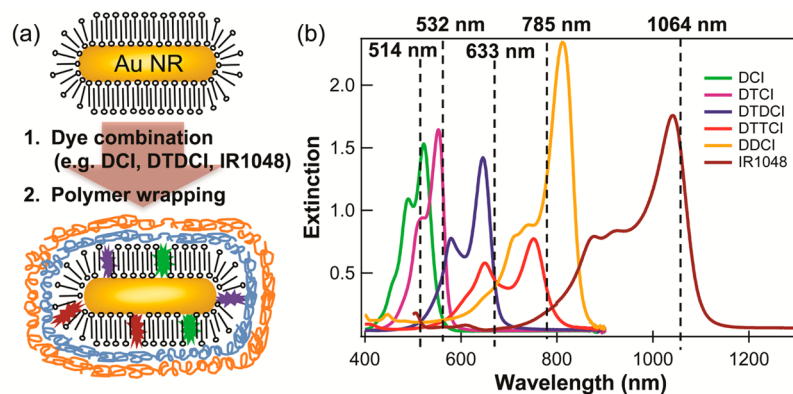
Figure 1. (a) Schematic outlining the preparation of universal SERRS tags (UST's). Different combinations of dyes can be sequestered in the CTAB bilayer simultaneously before polymer wrapping with multiple polyelectrolyte layers, starting with PSS as the base layer. (b) Extinction spectra of 10 μM dye solutions in 1 mM CTAB with the positions of the Raman laser excitation wavelengths used in this study are also shown.

commonly available laser excitation wavelengths. All of these dyes also have at least a partial spectral overlap with the LSPR extinction of the gold nanorod solution shown in Figure 2(a).

When preparing each NR−dye conjugate the relative nanorod and dye concentrations were kept constant at ~0.3 nM and 10 μM, respectively, and incubated overnight. Following PSS wrapping, the colloid was washed and resuspended in distilled water multiple times to ensure that all excess dye was removed. The extinction spectrum of each NR−dye combination is shown in the Supporting Information, Figure S3. Both blue and red shifts as well as dampening of the nanorod LSPR peak maximum at 815 nm were observed depending on the resonance overlap between the dye and NR.[22,32] The absence of peak splitting in any of the LSPR spectra, which is indicative of plasmon-exciton coupling,[32,33] is due to CTAB preventing dye molecule aggregates forming on the nanorod surface.[22] Bulk Raman spectra were then acquired for each nanorod−dye combination solution at 5 different laser excitation wavelengths (514, 532, 633, 785, 1064 nm) with each measurement normalized with respect to a cyclohexane standard (see Figures S4−S10, Supporting Information) to facilitate direct comparison. As expected, no single reporter dye exhibits strong Raman signals over such a wide excitation range and based on this analysis a combination of three dyes were subsequently selected to form the basis of the UST design. These were 1,1′-diethyl-2,2′-cyanine iodide (DCI), diethylthiadicarbocyanine iodide (DTDCI) and IR1048.

The extinction and Raman spectra of colloidal suspensions of UST's prepared with this three dye combination are shown in Figure 2. The fractional surface coverage of each dye on the nanorod surface depends on the relative bulk concentrations of the nanorods, CTAB and each dye present when mixed together. Recent work by us identified a maximum dye loading concentration of 50 μM for DTDCI without
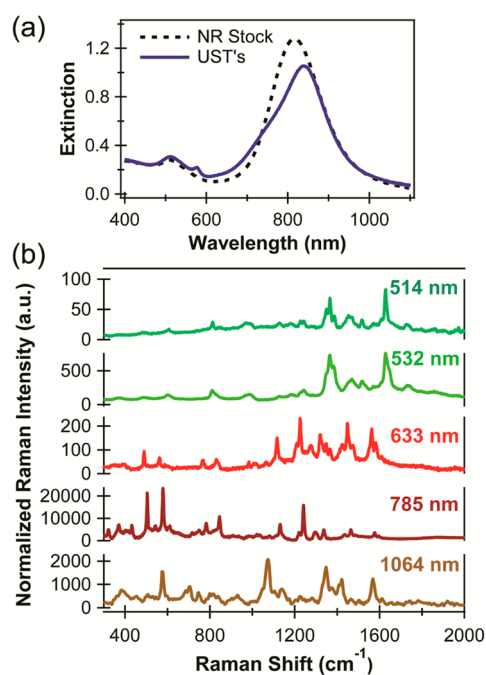

Figure 2. Optical characterization of universal SERRS tags prepared with 3 dyes (DCI, DTDCI, IR1048) present in the CTAB bilayer. (a) Extinction spectra of PSS-wrapped rods both with and without dye. The small peak at 577 nm in the UST spectrum is associated with DCI adsorbed on the NR surface. (b) Comparative Raman analysis of the same colloidal UST sample at different excitation wavelengths. Data has been baseline corrected and normalized with respect to the C_6H_{12} peak intensity at 1029 ($\pm$2) cm^{-1}.

causing colloidal destabilization at similar nanorod and CTAB concentrations.[22] As a result, the total combined dye concentration was fixed at 30 μM to reduce direct competition between different dye species for available surface adsorption sites. When investigating multiple dye addition, it was discovered that a successful UST preparation involved first introducing DCI and IR1048 to the NR stock solution followed by a time delay of 1 h before adding DTDCI and then leaving overnight to equilibrate. If all three dyes were introduced simultaneously, the higher affinity of DTDCI for
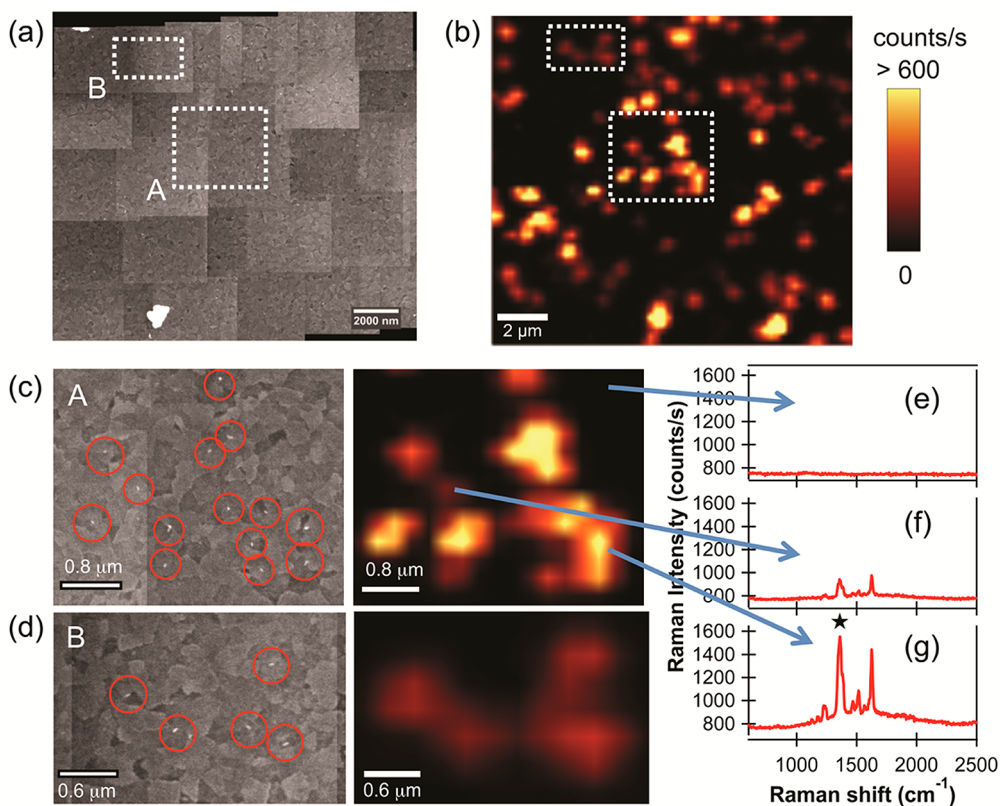
Figure 3. Correlated SEM and SERRS imaging on an ITO film coated glass slide. (a) SEM image obtained by stitching together high resolution images of smaller areas, along with (b) corresponding Raman image obtained for a confocal mapped area *circa* 14 μm × 13 μm. (c) Zoomed in views of selected area (box A) and (e−g) representative raw SERRS spectra from different surface regions. Analysis of the peak at 1360 cm^{-1} (denoted ★) following background subtraction was used to generate the Raman map with the brightest areas corresponding to peak intensities >600−1700$_{max}$ counts/s. (d) Magnified view of selected area (box B). Isolated nanorods are encircled. Raman data was obtained at 532 nm excitation, with an incident laser power of 0.6 mW, 1 s integration time and data acquired at 0.25 μm spatial steps.

the CTAB bilayer limited the partitioning of the other two dyes (see Figure S11, Supporting Information, for details). Instead, by using a staggered dye addition it is clear from the Raman spectra in Figure 2(b) that strong SERRS signals can be obtained simultaneously across all excitation wavelengths. This was achieved even though the relative contributions of both the LSPR and dye to the overall SERRS signal enhancement is strongly wavelength dependent.[22]

To date, very little work has been carried out on the controlled coadsorption of multiple Raman reporters onto the same nanoparticle surface. Le Ru *et al.* developed a bianalyte technique as proof of single molecule detection by SERS.[34] Faulds *et al.* have also reported the multiplexed detection of a mixture of five different individual dye labeled oligonucleotides conjugated to spherical silver nanoparticles, which were also then aggregated and excited at two wavelengths.[35] The normalized signal intensities in Figure 2(b) can be compared with Figures S4−S9 (Supporting Information) as both the NR and individual dye bulk concentrations are similar. This reveals that the SERRS intensity at 633 nm for the UST's is similar to that for DTDCI only but lower for DCI at 532 nm and IR1048 at 1064 nm, which

indicates that DTDCI has a ∼2-fold higher affinity for the CTAB bilayer. Since we have previously shown that the dye surface adsorption follows Langmuir isotherm behavior,[22] the relative signal intensities can be controlled *via* the total bulk dye concentration and adjusting the concentration ratio of each dye at a fixed NR concentration. For the UST's in Figure 2 further work was not necessary to increase the relative SERRS intensity at 532 nm to compensate for the lower surface affinity of DCI as there was sufficient reporter coverage to perform measurements at the single nanoparticle level.

Correlated Single Nanoparticle SERRS and SEM Surface Mapping. To clearly demonstrate that strong SERRS signals are obtained from single, nonaggregated, nanorod tags a series of measurements were performed where both confocal Raman and scanning electron microscopy (SEM) were used to map the same surface region where UST's were immobilized. This was achieved by attaching a reference grid onto an indium tin oxide (ITO) coated glass substrate which had been functionalized with a polyelectrolyte layer of opposite charge to that of the outer layer of the USTs described above (details in Supporting Information and Figure S12).

After a ~1 min exposure to colloidal solution, the glass substrate was rinsed with water and then dried, resulting in a low density particle surface coverage while avoiding additional drying-induced aggregation.[5]

Figure 3 compares SERRS and SEM maps of the same ~180 μm^2 area. The Raman measurements were performed first using 532 nm excitation and a 0.25 μm step size with the laser power kept low (0.6 mW) to ensure repeat scans could be carried out on the same area. Also shown in Figure 3(e−g) are representative raw spectra acquired at different locations. To generate the false color Raman maps, the peak intensity at 1360 cm^{-1} was calculated using a baseline corrected spectrum at each pixel. In order to directly visualize individual nanoparticles, a series of stepped high-resolution images were acquired using an environmental SEM and subsequently stitched together using an ImageJ plugin application[36] by taking advantage of the random patterning of the polycrystalline ITO layer.

When directly comparing the expanded areas highlighted in Figure 3(c,d) it can be clearly seen that there is a very strong correlation between areas of high Raman signal with individual nanoparticles present on the surface. The theoretical optical lateral resolution is ~360 nm at 532 nm excitation; however, the correlated maps indicate that the actual spot size is larger than this, as expected. The data in Figure 3(d) further highlights that SERRS signals from individual particles can be readily measured and that the effective excitation spot width at 532 nm must be less than 600 nm.

The dual mapping approach also enabled us to establish the percentage of nanoparticles that are SERRS active by locating every nanorod and comparing the optical signal at the same location. The measurement acquisition settings and lateral step size used in Figure 3 were selected to help ensure that signal from every Raman-active particle within the mapped area would be collected. A repeat SEM/SERRS map was also created for another surface area of similar size on the same substrate resulting in over 300 nanorods analyzed of which a minimum of 92% were SERRS-active. This significant result is due to the combined resonance enhancement of the dye reporter and nanorod plus good control of the NR surface chemistry and avoiding the added complication of an induced aggregation step. For comparison, a number of studies involving quasi-spherical metallic nanoparticles have reported SERS yields of ~70% and higher, but only for aggregated colloidal systems.[4,37−40]

Analysis of the surface maps when only an individual rod is present in the beam focus reveals that the 1360 cm^{-1} peak intensity varies from 145 to 450 counts/s with a mean value of 269 counts/s. In Figure 3(f), the weaker signal (155 counts/s) is clearly obtained from a single particle, while the larger signal (690 counts/s) in Figure 3(g) indicates that there are at least 2 isolated nanorods within the beam focus at this region. Reasons for the range in single nanoparticle intensities include that there is an intrinsic variation in rod length and thus number of reporter molecules at the single particle level and it is likely that the nanorod and excitation beam will not be optimally overlapping for maximum signal at each step position. In addition, the incident light is polarized at a fixed angle (no polarization optics are present in the detection path) and the relative orientation of the rod transverse and longitudinal plasmon resonances with respect to the incident polarized light is another likely source of signal variation.

The good signal-to-noise of the Raman spectra demonstrated in Figure 3 combined with sub-mW laser powers and 1 s acquisition times compares favorably with recent SERS studies of individual particles[10,12] and clusters[16,20] as well as a report on the large Raman enhancement of dye aggregates formed within carbon nanotubes.[41] Since a mixed layer of CTAB and three different dyes is formed on the nanorod surface, better understanding of this composition is required to report a meaningful Raman enhancement factor compared to an approach where full monolayer coverage of a single reporter molecule is assumed. Measuring instead the differential Raman cross-section of an individual rod−dye conjugate at various excitation wavelengths represents a promising route to quantify the brightness of the UST's and requires the development of new methodologies to achieve this (e.g., refs 41, 42). Regardless of these challenges, the data presented demonstrates that Raman spectra can be readily obtained at very high yields from individual, nonaggregated particles <50 nm in size.

Multiwavelength SERRS Mapping. Repeat measurements were also performed where the same substrate area was mapped using a range of multiple laser excitation wavelengths coupled to an imaging spectrometer. Figure 4 compares false color images generated at 532, 633, and 785 nm excitation on a glass slide featuring a surface-etched reference grid and a low particle coverage density. Each laser was kept to a similarly low incident power (0.6 mW), which allowed the same surface area to be mapped multiple times with no noticeable photodegradation, while still obtaining strong Raman signals at the single nanoparticle level at each available excitation wavelength. Comparison of the SERRS maps and representative raw data spectra indicate both poorer signal-to-noise and lower spatial resolution as the excitation wavelength is increased. This is partly because the diffraction limited spot size at 785 nm is ~60% larger than at 532 nm, which resulted in a lower incident power density. These results indicate that attempting similar mapping measurements at 1064 nm would be even more challenging. Only bulk measurements at 1064 nm were available to us, however, the relative intensities of the normalized signals in Figure 2 (which is higher for 1064 nm than at
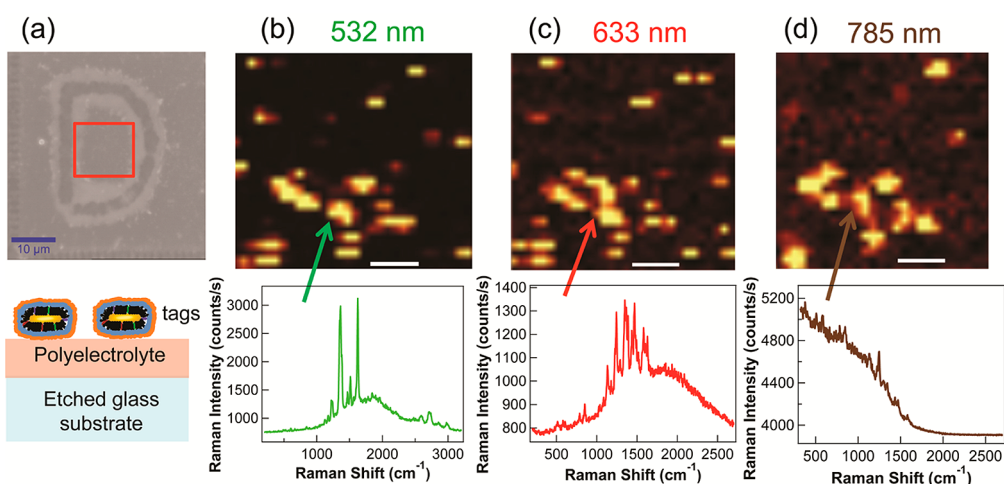
Figure 4. (a) Optical bright-field image and defined region of interest mapped. False color images of mapped area at the following laser excitations: (b) 532 nm (laser power 0.6 mW), (c) 633 nm (laser power 0.6 mW) and (d) 785 nm (laser power 0.7 mW). All data was obtained using a 0.5 s integration time and at 0.5 μm spatial steps. White scale bars = 3 μm. The Raman maps were created from max/min intensity analysis in peak regions at 1360 cm^{-1} for 532 nm and at 1245 cm^{-1} for both 633 and 785 nm. The max intensity areas in each map correspond to peak signals >220$-$1830$_{max}$ (532 nm), >45$-$330$_{max}$ (633 nm) and >25$-$238$_{max}$ (785 nm) counts/s.

633 or 532 nm) suggests that measurements at the single particle level at 1064 nm could be achieved. It is also important to point out that the spectra in Figure 2 were acquired with different spectrometers from that used in Figure 4 (and later in Figure 6) and that the LSPR of individual surface-immobilized nanorods in air will be considerably different from the water-suspended bulk ensemble measurements. These factors could also play a role in the relative SERRS intensities obtained at different excitation wavelengths.

The particular UST's described here were designed specifically to give high signal intensities across a wide excitation range from 514$-$1064 nm. However, improved imaging performance across the 532$-$785 nm range can be obtained by using a different dye combination. An example is shown in the Supporting Information (Figure S13) for tags prepared using a 1 DCI:2 DTDCI dye ratio. Improved correlation between the Raman maps signal intensities at different excitation wavelengths was obtained due to a relatively higher fractional surface coverage of DTDCI on the nanorod surface and the absence of the IR1048 dye.

Multimodal Optical Single Cell Mapping. In a final set of experiments we demonstrate the *in vitro* bioimaging efficacy of UST's for multiwavelength single cell imaging measurements using Raman, fluorescence and dark-field optical modalities. This was performed by incubating the tags with primary (bone-marrow derived) mouse dendritic cells (DC's), which, due to their role in the initiation of the immune response, are likely to be important cells for the development of new technologies using nanoparticle delivery, such as therapeutic targeting and stimulating immunity.[43,44] First, to confirm whether the tags affect DC viability, cells were analyzed after incubation with various concentrations of UST's
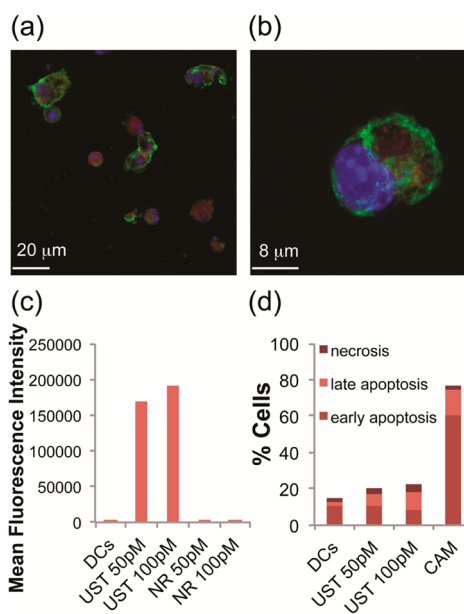

Figure 5. Demonstration that nanorod$-$PSS-PDDAC dye conjugates do not significantly affect dendritic cell viability. Confocal fluorescent images with nuclei staining (DAPI, blue; 405 nm excitation), Cholera Toxin Subunit B (Recombinant), Alexa Fluor 488 Conjugate staining (cell membrane shown in green, 488 nm excitation) and nanoparticle tags in red (633 nm excitation) after overnight incubation at (a) 100 pM and (b) 10 pM tag concentration. Flow cytometry data showing (c) mean fluorescence intensity at 633 nm of cells incubated with UST's for 2 h and also polymer wrapped nanorod controls, NR, with no reporter dyes. Data shows uptake quantification is possible for UST's using fluorescence. Shown in (d) is the percentage of cells undergoing early apoptosis (Annexin-V positive, Propidium Iodide negative), late apoptosis (Annexin-V and Propidium Iodide positive) and necrosis (Propidium Iodide positive, Annexin-V negative) measured by flow cytometry after 24 h incubation with UST's at 50 and 100 pM in the cell suspension and compared with nonstimulated cells (DCs) and cells incubated with camptothecin only (CAM). Data shows that the nanoparticle probes show no significant toxicity even after 24 h-long incubations at high concentrations.
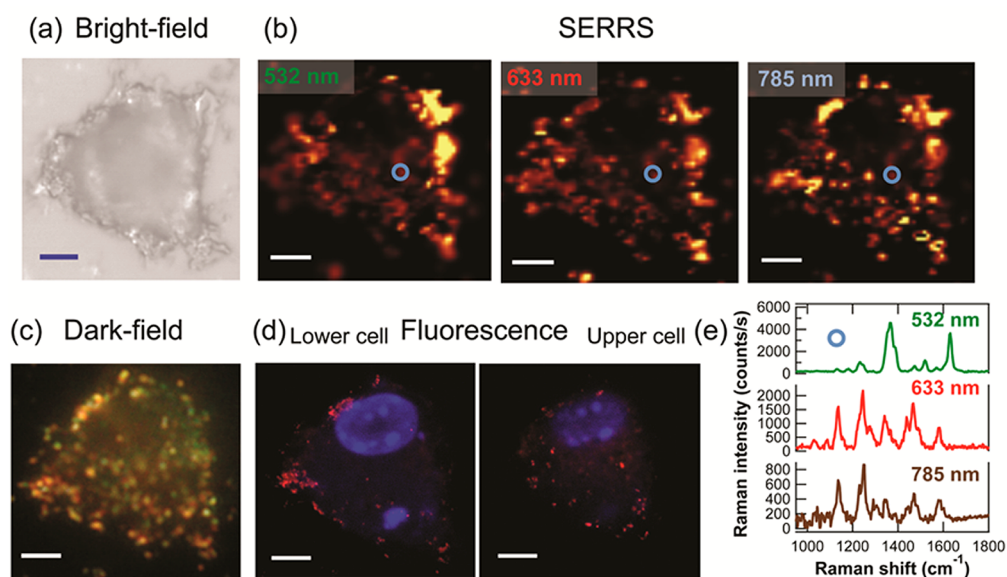
Figure 6. Multimodal optical imaging of a dendritic cell which was fixed after incubation with 100 pM UST's for 4 h. (a) Bright-field image and (c) transmission dark-field image of the area mapped repeatedly using (b) a Raman confocal microscope at three different excitation wavelengths (532, 633, and 785 nm) and (d) confocal fluorescence images of lower and upper regions of a vertical image stack (blue, 405 nm; red, 633 nm excitation). (e) Representative SERRS spectra (background corrected) from within the circled region in each of the Raman maps. All SERRS data were obtained using a 0.5 s integration time and at 0.4 μm spatial steps. The Raman maps were created from max/min intensity analysis in peak regions at 1360 cm^{-1} for 532 nm (laser power 0.54 mW) and at 1245 cm^{-1} for both 633 and 785 nm (0.66 and 0.73 mW respectively). The brightest intensities in each map correspond to signals >18 000−42 000$_{max}$ (532 nm), >5000−8900$_{max}$ (633 nm), >2500−6000$_{max}$ (785 nm) counts/s. All scale bars = 5 μm.

using flow cytometry to quantify apoptotic (Annexin-FITC) and necrotic (Propidium Iodide) cells. UST uptake and intracellular localization was also observed using confocal fluorescence imaging. Cells readily internalized UST's across a range of doses and this was detectable by both confocal imaging (Figure 5a,b) and flow cytometry (Figure 5c,d). It is well-established that freely suspended CTAB is cytotoxic;[45,46] however, our results agree with several recent examples in the literature where polyelectrolyte wrapped nanorods (with the stabilizing CTAB bilayer still present) have been found to not have a significant impact on cell viability.[45,47,48] The formation of a surrounding layer or corona of serum proteins around the polymer-coated nanoparticle is also an important part of a nonspecific cell uptake mechanism.[45,49,50]

The potential of UST's as imaging contrast agents for intracellular mapping across a range of excitation wavelengths is highlighted in Figure 6, where the same cell was repeatedly mapped in separate confocal Raman and fluorescent microscopes following incubation with UST's. Measurements of control cells that have not been exposed to nanoparticles are shown in the Supporting Information (Figure S14), where no characteristic Raman peaks associated with intracellular molecules[51] were observed at the relatively low laser powers and integration times used here. The fluorescence signal at 633 nm is due to the DTDCI dye, which is not completely quenched at the single nanorod level despite close proximity to the metal surface (within the ∼4−5 nm thick CTAB bilayer); however, no detectable fluorescent signal was obtained when exciting at 532 nm.

All of the SERRS maps in Figure 6(b) display localized areas of varying signal intensity that is associated with different UST densities. Relative differences between maps at each excitation wavelength are due to a number of factors such as laser spot size and, in particular, the relative position and depth of the focal plane within the cell. Repeat fluorescence and Raman maps were acquired at different focal depths for a number of cells to confirm UST internalization as well as signals proximate to the membrane. The lateral and depth resolution of the fluorescence microscope is better than that of the Raman microscope and two fluorescent image stacks from the upper and lower cell regions are presented in Figure 6(d) with the position of the cell nuclei also defined by DAPI staining and 405 nm excitation. A simple visual comparison between the dark-field, SERRS and fluorescence images demonstrate the absence of particles within the cell nucleus, which is consistent with previous reports of nonspecific (nontargeted) gold nanoparticle uptake mechanisms.[52] Also, a number of correlative features can be observed between images, and Figure S15 (Supporting Information) shows an expanded view of the region around where the representative spectra are presented in Figure 6(e). It is also interesting to note that the areas of the brightest fluorescence intensity do not always correlate with the brightest SERRS signal. Further studies are now currently underway aimed at using the

UST's to achieve dynamic correlative imaging and spectroscopy measurements across multiple modalities at the single nanoparticle level in complex environments.

CONCLUSION

In this article, we have introduced the concept of a universal SERRS tag (UST) composed of individual, nonaggregated, gold nanorod/multidye conjugates capable of producing signals over a wide range of common excitation wavelengths (514−1064 nm). Key to the successful preparation of these tags is the well-controlled sequestering of similarly structured dyes within the stabilizing CTAB bilayer that surrounds the nanorod structure as well as avoiding the need for a particle aggregation step. In addition, the polyelectrolyte wrapping of the NR−dye conjugates imparts a long colloidal shelf life and provides an established platform for further surface functionalization. Having demonstrated that individual nanorod−dye conjugates are readily SERRS active, further investigations are currently underway involving *in situ* kinetic measurements of dye assembly on individual nanorods to further understand and characterize the nanorod−dye interaction and quantify the single nanoparticle brightness. It is very likely that the 514−1064 nm window used here can be further extended to both longer and shorter wavelengths. However, this requires investigating the relative importance of the degree of spectral overlap between the nanorod LSPR and each dye as well as end *versus* side surface adsorption sites on the nanorod and the absolute density of dye molecules. We envision that the ability to readily tailor the spectral profile, brightness and active optical window of individual particles will be valuable for a wide range of applications involving single particle tracking and image colocalization in biological environments such as drug delivery and disease detection.

EXPERIMENTAL SECTION

Chemicals. Cetyltrimethylammonium bromide (CTAB), hydrogen tetrachloroaurate ($HAuCl_4$), ascorbic acid, silver nitrate ($AgNO_3$), sodium borohydride ($NaBH_4$), sodium citrate tribasic dihydrate, 1,1′-diethyl-2,2′-cyanine iodide (DCI), 1,1′-diethyl-4,4′-dicarbocyanine iodide (DDCI), 3,3′-diethylthiacarbocyanine iodide (DTCI), 3,3′-diethylthiatricarbocyanine iodide (DTTCI), 3′,3′-diethylthiadicarbocyanine iodide (DTDCI), 1-butyl-2-[2-[3-[(1-butyl-6-chlorobenz[cd]indol-2(1H)-ylidene)ethylidene]-2-chloro-1-cyclohexen-1-yl]ethenyl]-6-chlorobenz[cd]indolium tetrafluoroborate (IR1048), poly(sodium 4-styrenesulfonate) (PSS) MW ∼70 000, sodium chloride (NaCl), poly(diallyldimethylammonium chloride) (PDDAC) MW ≤ 100 000, and cyclohexane were all purchased from Sigma-Aldrich and used as received. All solutions were prepared using Millipore water.

UST Synthesis. Gold nanorods were synthesized with the reaction volume scaled up to 1 L followed by repeated (3×) centrifugation and resuspension in 1 mM CTAB as described previously[22] and also in the Supporting Information. The final stock solution prior to dye addition had an OD of 1.3, which is ∼0.26 nM based on an extinction coefficient of 5 × 10^9 M^{-1} cm^{-1} at the λ_{max} of the longitudinal LSPR.[53] For each individual dye−nanorod combination, 1 M stock solutions of dye were prepared in methanol, and further diluted in Millipore water to 100 μM immediately prior to mixing an aliquot with the nanorods to give a bulk dye concentration of 10 μM. For the 3-dye UST's, 4 mL each of 100 μM DCI and IR1048 were premixed and added to 40 mL of NR solution. Four milliliters of DTDCI solution were then introduced either along with DCI and IR1048 (*i.e.*, 0 h delay) or following a 1 or 14 h equilibration of these dyes with the NRs. The nanorod−dye conjugate was polymer wrapped by slowly adding 8 mL of 10 mg/mL PSS in 5 mM NaCl to a 40 mL aliquot while rapidly stirring. The samples were then centrifuged and resuspended in water five times to ensure the removal of excess dyes from the solution. Subsequent PDDAC wrapping, centrifugation and resuspension (2×) was performed using the same conditions as for PSS coating.

Bulk Raman Measurements. Four different instruments were used covering 514, 532, 633, 785, and 1064 nm excitation with details provided in the Supporting Information. The intensities of the bulk spectra were normalized with respect to the 1029 (±2) cm^{-1} cyclohexane peak acquired from a neat solution under identical conditions. A signal collection time of 10 s per spectra was used throughout. All spectra were processed and background corrected using Grams/AI software (version 7.0).

Raman Mapping. Confocal Raman imaging in Figures 4 and 6 was carried out using a WITec Alpha300 R instrument with 532, 633, and 785 nm excitation lasers available. All maps were acquired using a 100× objective (Olympus MPlan, NA = 0.9) and additional acquisition details are described in each figure caption. WITec project 2.10 software was used for data processing of all Raman maps. Correlated single nanorod measurements were performed using an environmental FEI Quanta 250 SEM operating in low vacuum mode. An ITO coated glass slide [Sigma-Aldrich] functionalized with a PSS layer was used as a substrate upon which a reference finder grid was also immobilized (see Supporting Information and Figure S12 for further details).

Dendritic Cell−UST Interactions. Dendritic cells (DC's) were obtained from BALB/c mice as described previously.[54] Both FACS and confocal fluorescence imaging measurements were performed.

FACS Measurements. DC's were diluted to obtain a 5 × 10^5 cells/mL concentration in complete RPMI (RPMI 1640 with 10% FCS, 100 U/mL penicillin, 100 μg/mL streptomycin, 2 mM L-glutamine [Life Technologies, UK]). The cells were then replated into two 24-well Costar plates [Corning, USA] (0.5 mL/well) and incubated with (i) nothing added; (ii) 50 pM USTs; (iii) 100 pM USTs; or (iv) camptothecin (0.5 μL of 10 mM stock per 1 mL of cell suspension). Camptothecin [Sigma-Aldrich, UK] is an apoptosis inducer, used here as a positive control for apoptosis. Samples were then left to incubate at 37 °C and 5% CO_2 and harvested at 2, 4, and 24 h. Samples were stained using an Annexin-V(FITC) and Propidium Iodide kit [eBioscience, UK] according to manufacturer's instructions and analyzed using a BD FACSCanto equipment and BD FACSDiva software.

Confocal Fluorescence Imaging of Nanoparticle Uptake (Figure 5a,b). DCs were replated at 5 × 10^4 cells/mL into one 8-well glass slide [Lab-Tek II Chamber Slide, Nunc] and duplicate wells were inoculated with 1 pM, 10 pM and 100 pM UST's (0.5 mL/well). These samples were left to incubate for 24 h, stained with Cholera Toxin Subunit B (Recombinant) Alexa Fluor 488 Conjugate [Life Technologies, UK] for 10 min and fixed with 4% paraformaldehyde [Sigma-Aldrich, UK]. Cells were then gently washed with 0.5X HBSS [Life Technologies, UK] and a coverslip mounted onto the slide using VectaShield mounting medium with DAPI [Vector Laboratories, UK].

Confocal Fluorescence and Raman Imaging of Cells (Figures 6, S14, S15). DC's at 5 × 10^4 cells/mL were replated onto 35 mm Grid-50 μ-dishes [Ibidi, Germany] (0.5 mL/dish) and left to

incubate overnight at 37 °C and 5% CO_2. UST's were then added to one of the cell dishes at an approximate final concentration of 100 pM in the cell suspension and the dishes incubated for 4 h. Cells were subsequently fixed and washed as above and samples left to air-dry before Raman mapping. Next, for confocal fluorescence mapping, coverslips were mounted onto the cell samples using VectaShield mounting medium with DAPI. Samples were then fluorescence mapped (at 405 and 633 nm wavelengths), with z-stacks obtained for each analyzed cell at 0.5 μm steps and two-frame average acquisition. Finally, dark-field imaging in transmission was performed using a Nikon Eclipse LV100 microscope equipped with an oil dark-field condenser, a 100× (NA = 0.9) objective and a Nikon D50 camera.

Conflict of Interest: The authors declare no competing financial interest.

Supporting Information Available: Additional experimental details on nanorod preparation and bulk and confocal Raman measurements. Figures S1–S15 feature additional electron microscopy, extinction and Raman characterization of different nanorod—dye combinations as well as supporting mapped images of dendritic cells. This material is available free of charge *via* the Internet at http://pubs.acs.org.

REFERENCES AND NOTES

1. Wang, Y.; Yan, B.; Chen, L. SERS Tags: Novel Optical Nanoprobes for Bioanalysis. *Chem. Rev.* **2013**, *113*, 1391–1428.
2. McNay, G.; Eustace, D.; Smith, W. E.; Faulds, K.; Graham, D. Surface-Enhanced Raman Scattering (SERS) and Surface-Enhanced Resonance Raman Scattering (SERRS): A Review of Applications. *Appl. Spectrosc.* **2011**, *65*, 825–837.
3. Kleinman, S. L.; Frontiera, R. R.; Henry, A. I.; Dieringer, J. A.; Van Duyne, R. P. Creating, Characterizing, and Controlling Chemistry with SERS Hot Spots. *Phys. Chem. Chem. Phys.* **2013**, *15*, 21–36.
4. Wustholz, K. L.; Henry, A. I.; McMahon, J. M.; Freeman, R. G.; Valley, N.; Piotti, M. E.; Natan, M. J.; Schatz, G. C.; Duyne, R. P. V. Structure-Activity Relationships in Gold Nanoparticle Dimers and Trimers for Surface-Enhanced Raman Spectroscopy. *J. Am. Chem. Soc.* **2010**, *132*, 10903–10910.
5. McLintock, A.; Hunt, N.; Wark, A. W. Controlled Side-by-Side Assembly of Gold Nanorods and Dye Molecules into Polymer-Wrapped SERRS-Active Clusters. *Chem. Commun.* **2011**, *47*, 3757–3759.
6. Wang, Y.; Schluecker, S. Rational Design and Synthesis of SERS Labels. *Analyst* **2013**, *138*, 2224–2238.
7. Tay, L. L.; Hulse, J.; Kennedy, D.; Pezacki, J. P. Surface-Enhanced Raman and Resonant Rayleigh Scatterings from Adsorbate Saturated Nanoparticles. *J. Phys. Chem. C* **2010**, *114*, 7356–7363.
8. Rodriguez-Lorenzo, L.; Alvarez-Puebla, R. A.; Pastoriza-Santos, I.; Mazzucco, S.; Stephan, O.; Kociak, M.; Liz-Marzan, L. M.; Garcia de Abajo, F. J. Zeptomol Detection through Controlled Ultrasensitive Surface-Enhanced Raman Scattering. *J. Am. Chem. Soc.* **2009**, *131*, 4616–4618.
9. Talley, C. E.; Jackson, J. B.; Oubre, C.; Grady, N. K.; Hollars, C. W.; Lane, S. M.; Huser, T. R.; Nordlander, P.; Halas, N. J. Surface-Enhanced Raman Scattering from Individual Au Nanoparticles and Nanoparticle Dimer Substrates. *Nano Lett.* **2005**, *5*, 1569–1574.
10. Aldeanueva-Potel, P.; Carbo-Argibay, E.; Pazos-Perez, N.; Barbosa, S.; Pastoriza-Santos, I.; Alvarez-Puebla, R. A.; Liz-Marzan, L. M. Spiked Gold Beads as Substrates for Single-Particle SERS. *ChemPhysChem* **2012**, *13*, 2561–2565.
11. Rycenga, M.; Camargo, P. H. C.; Li, W.; Moran, C. H.; Xia, Y. Understanding the SERS Effects of Single Silver Nanoparticles and Their Dimers, One at a Time. *J. Phys. Chem. Lett.* **2010**, *1*, 696–703.
12. Mulvihill, M. J.; Ling, X. Y.; Henzie, J.; Yang, P. Anisotropic Etching of Silver Nanoparticles for Plasmonic Structures Capable of Single-Particle SERS. *J. Am. Chem. Soc.* **2010**, *132*, 268–274.
13. Lin, H. X.; Li, J. M.; Liu, B. J.; Liu, D. Y.; Liu, J.; Terfort, A.; Xie, Z. X.; Tian, Z. Q.; Ren, B. Uniform Gold Spherical Particles for Single-Particle Surface-Enhanced Raman Spectroscopy. *Phys. Chem. Chem. Phys.* **2013**, *15*, 4130–4135.
14. Liang, H.; Li, Z.; Wang, W.; Wu, Y.; Xu, H. Highly Surface-Roughened "Flower-Like" Silver Nanoparticles for Extremely Sensitive Substrates of Surface-Enhanced Raman Scattering. *Adv. Mater.* **2009**, *21*, 4614–4618.
15. Kleinman, S. L.; Sharma, B.; Blaber, M. G.; Henry, A. I.; Valley, N.; Freeman, R. G.; Natan, M. J.; Schatz, G. C.; Van Duyne, R. P. Structure Enhancement Factor Relationships in Single Gold Nanoantennas by Surface-Enhanced Raman Excitation Spectroscopy. *J. Am. Chem. Soc.* **2013**, *135*, 301–308.
16. Xie, H.-n.; Larmour, I. A.; Tileli, V.; Koh, A. L.; McComb, D. W.; Faulds, K.; Graham, D. Deciphering Surface Enhanced Raman Scattering Activity of Gold Nanoworms through Optical Correlations. *J. Phys. Chem. C* **2011**, *115*, 20515–20522.
17. Pazos-Perez, N.; Wagner, C. S.; Romo-Herrera, J. M.; Liz-Marzan, L. M.; Garcia de Abajo, F. J.; Wittemann, A.; Fery, A.; Alvarez-Puebla, R. A. Organized Plasmonic Clusters with High Coordination Number and Extraordinary Enhancement in Surface-Enhanced Raman Scattering (SERS). *Angew. Chem., Int. Ed.* **2012**, *51*, 12688–12693.
18. Rycenga, M.; Xia, X.; Moran, C. H.; Zhou, F.; Qin, D.; Li, Z. Y.; Xia, Y. Generation of Hot Spots with Silver Nanocubes for Single-Molecule Detection by Surface-Enhanced Raman Scattering. *Angew. Chem., Int. Ed.* **2011**, *50*, 5473–5477.
19. Cecchini, M. P.; Wiener, A.; Turek, V. A.; Chon, H.; Lee, S.; Ivanov, A. P.; McComb, D. W.; Choo, J.; Albrecht, T.; Maier, S. A.; et al. Rapid Ultrasensitive Single Particle Surface-Enhanced Raman Spectroscopy Using Metallic Nanopores. *Nano Lett.* **2013**, *13*, 4602–4609.
20. Steinigeweg, D.; Schütz, M.; Schlücker, S. Single Gold Trimers and 3D Superstructures Exhibit a Polarization-Independent SERS Response. *Nanoscale* **2013**, *5*, 110–113.
21. Osberg, K. D.; Rycenga, M.; Harris, N.; Schmucker, A. L.; Langille, M. R.; Schatz, G. C.; Mirkin, C. A. Dispersible Gold Nanorod Dimers with Sub-5 nm Gaps as Local Amplifiers for Surface-Enhanced Raman Scattering. *Nano Lett.* **2012**, *12*, 3828–3832.
22. McLintock, A.; Lee, H. J.; Wark, A. W. Stabilized Gold Nanorod-Dye Conjugates with Controlled Resonance Coupling Create Bright Surface-Enhanced Resonance Raman Nanotags. *Phys. Chem. Chem. Phys.* **2013**, *15*, 18835–18843.
23. Sivapalan, S. T.; DeVetter, B. M.; Yang, T. K.; van Dijk, T.; Schulmerich, M. V.; Carney, P. S.; Bhargava, R.; Murphy, C. J. Off-Resonance Surface-Enhanced Raman Spectroscopy from Gold Nanorod Suspensions as a Function of Aspect Ratio: Not What We Thought. *ACS Nano* **2013**, *7*, 2099–2105.
24. Lee, A.; Ahmed, A.; Dos Santos, D. P.; Coombs, N.; Park, J. I.; Gordon, R.; Brolo, A. G.; Kumacheva, E. Side-by-Side Assembly of Gold Nanorods Reduces Ensemble-Averaged SERS Intensity. *J. Phys. Chem. C* **2012**, *116*, 5538–5545.
25. Lee, A.; Andrade, G. F. S.; Ahmed, A.; Souza, M. L.; Coombs, N.; Tumarkin, E.; Liu, K.; Gordon, R.; Brolo, A. G.; Kumacheva, E. Probing Dynamic Generation of Hot-Spots in Self-Assembled Chains of Gold Nanorods by Surface-Enhanced Raman Scattering. *J. Am. Chem. Soc.* **2011**, *133*, 7563–7570.
26. Huang, X.; El-Sayed, I. H.; Qian, W.; El-Sayed, M. A. Cancer Cells Assemble and Align Gold Nanorods Conjugated to Antibodies to Produce Highly Enhanced, Sharp, and Polarized Surface Raman Spectra: A Potential Cancer Diagnostic Marker. *Nano Lett.* **2007**, *7*, 1591–1597.

27. von Maltzahn, G.; Centrone, A.; Park, J.-H.; Ramanathan, R.; Sailor, M. J.; Hatton, T. A.; Bhatia, S. N. SERS-Coded Gold Nanorods as a Multifunctional Platform for Densely Multiplexed Near-Infrared Imaging and Photothermal Heating. *Adv. Mater.* **2009**, *21*, 3175–3180.

28. Nordlander, P.; Oubre, C.; Prodan, E.; Li, K.; Stockman, M. I. Plasmon Hybridization in Nanoparticle Dimers. *Nano Lett.* **2004**, *4*, 899–903.

29. Willingham, B.; Brandl, D. W.; Nordlander, P. Plasmon Hybridization in Nanorod Dimers. *Appl. Phys. B: Lasers Opt.* **2008**, *93*, 209–216.

30. Lee, S.; Chon, H.; Yoon, S. Y.; Lee, E. K.; Chang, S. I.; Lim, D. W.; Choo, J. Fabrication of SERS-Fluorescence Dual Modal Nanoprobes and Application to Multiplex Cancer Cell Imaging. *Nanoscale* **2012**, *4*, 124–129.

31. Zhang, Y.; Qian, J.; Wang, D.; Wang, Y.; He, S. Multifunctional Gold Nanorods with Ultrahigh Stability and Tunability for *In Vivo* Fluorescence Imaging, SERS Detection, and Photodynamic Therapy. *Angew. Chem., Int. Ed.* **2013**, *52*, 1148–1151.

32. Ni, W. H.; Yang, Z.; Chen, H. J.; Li, L.; Wang, J. F. Coupling between Molecular and Plasmonic Resonances in Freestanding Dye-Gold Nanorod Hybrid Nanostructures. *J. Am. Chem. Soc.* **2008**, *130*, 6692–6693.

33. Fofang, N. T.; Park, T.-H.; Neumann, O.; Mirin, N. A.; Nordlander, P.; Halas, N. J. Plexcitonic Nanoparticles: Plasmon-Exciton Coupling in Nanoshell-J-Aggregate Complexes. *Nano Lett.* **2008**, *8*, 3481–3487.

34. Le Ru, E. C.; Galloway, C.; Etchegoin, P. G. On the Connection between Optical Absorption/Extinction and SERS Enhancements. *Phys. Chem. Chem. Phys.* **2006**, *8*, 3083–3087.

35. Faulds, K.; McKenzie, F.; Smith, W. E.; Graham, D. Quantitative Simultaneous Multianalyte Detection of DNA by Dual-Wavelength Surface-Enhanced Resonance Raman Scattering. *Angew. Chem., Int. Ed.* **2007**, *46*, 1829–1831.

36. Preibisch, S.; Saalfeld, S.; Tomancak, P. Globally Optimal Stitching of Tiled 3d Microscopic Image Acquisitions. *Bioinformatics* **2009**, *25*, 1463–1465.

37. Wark, A. W.; Stokes, R. J.; Darby, S. B.; Smith, W. E.; Graham, D. Dynamic Imaging Analysis of SERS -Active Nanoparticle Clusters in Suspension. *J. Phys. Chem. C* **2010**, *114*, 18115–18120.

38. Laurence, T. A.; Braun, G.; Talley, C.; Schwartzberg, A.; Moskovits, M.; Reich, N.; Huser, T. Rapid, Solution-Based Characterization of Optimized SERS Nanoparticle Substrates. *J. Am. Chem. Soc.* **2009**, *131*, 162–169.

39. Sebba, D. S.; Watson, D. A.; Nolan, J. P. High Throughput Single Nanoparticle Spectroscopy. *ACS Nano* **2009**, *3*, 1477–1484.

40. Goddard, G.; Brown, L. O.; Habbersett, R.; Brady, C. I.; Martin, J. C.; Graves, S. W.; Freyer, J. P.; Doorn, S. K. High-Resolution Spectral Analysis of Individual SERS-Active Nanoparticles in Flow. *J. Am. Chem. Soc.* **2010**, *132*, 6081–6090.

41. Gaufres, E.; Tang, N. Y.-W.; Lapointe, F.; Cabana, J.; Nadon, M. A.; Cottenye, N.; Raymond, F.; Szkopek, T.; Martel, R. Giant Raman Scattering from J-Aggregated Dyes inside Carbon Nanotubes for Multispectral Imaging. *Nat. Photonics* **2014**, *8*, 72–78.

42. Bohn, J. E.; Etchegoin, P. G.; Le Ru, E. C.; Xiang, R.; Chiashi, S.; Maruyama, S. Estimating the Raman Cross Sections of Single Carbon Nanotubes. *ACS Nano* **2010**, *4*, 3466–3470.

43. Reddy, S. T.; Swartz, M. A.; Hubbell, J. A. Targeting Dendritic Cells with Biomaterials: Developing the Next Generation of Vaccines. *Trends Immunol.* **2006**, *27*, 573–579.

44. Paulis, L. E.; Mandal, S.; Kreutz, M.; Figdor, C. G. Dendritic Cell-Based Nanovaccines for Cancer Immunotherapy. *Curr. Opin. Immunol.* **2013**, *25*, 389–395.

45. Alkilany, A. M.; Nagaria, P. K.; Hexel, C. R.; Shaw, T. J.; Murphy, C. J.; Wyatt, M. D. Cellular Uptake and Cytotoxicity of Gold Nanorods: Molecular Origin of Cytotoxicity and Surface Effects. *Small* **2009**, *5*, 701–708.

46. Cheung, K. L.; Chen, H.; Chen, Q.; Wang, J.; Ho, H. P.; Wong, C. K.; Kong, S. K. Ctab-Coated Gold Nanorods Elicit Allergic

47. Response through Degranulation and Cell Death in Human Basophils. *Nanoscale* **2012**, *4*, 4447–4449.

47. Xu, L. G.; Liu, Y.; Chen, Z. Y.; Li, W.; Wang, L. M.; Wu, X. C.; Ji, Y. L.; Zhao, Y. L.; Ma, L. Y.; Shao, Y. M.; *et al.* Surface-Engineered Gold Nanorods: Promising DNA Vaccine Adjuvant for Hiv-1 Treatment. *Nano Lett.* **2012**, *12*, 2003–2012.

48. Hauck, T. S.; Ghazani, A. A.; Chan, W. C. W. Assessing the Effect of Surface Chemistry on Gold Nanorod Uptake, Toxicity, and Gene Expression in Mammalian Cells. *Small* **2008**, *4*, 153–159.

49. Walkey, C. D.; Olsen, J. B.; Guo, H.; Emili, A.; Chan, W. C. W. Nanoparticle Size and Surface Chemistry Determine Serum Protein Adsorption and Macrophage Uptake. *J. Am. Chem. Soc.* **2012**, *134*, 2139–2147.

50. Qiu, Y.; Liu, Y.; Wang, L. M.; Xu, L. G.; Bai, R.; Ji, Y. L.; Wu, X. C.; Zhao, Y. L.; Li, Y. F.; Chen, C. Y. Surface Chemistry and Aspect Ratio Mediated Cellular Uptake of Au Nanorods. *Biomaterials* **2010**, *31*, 7606–7619.

51. McAughtrie, S.; Lau, K.; Faulds, K.; Graham, D. 3d Optical Imaging of Multiple SERS Nanotags in Cells. *Chem. Sci.* **2013**, *4*, 3566–3572.

52. Gregas, M. K.; Scaffidi, J. P.; Lauly, B.; Vo-Dinh, T. Surface-Enhanced Raman Scattering Detection and Tracking of Nanoprobes: Enhanced Uptake and Nuclear Targeting in Single Cells. *Appl. Spectrosc.* **2010**, *64*, 858–866.

53. Orendorff, C. J.; Murphy, C. J. Quantitation of Metal Content in the Silver-Assisted Growth of Gold Nanorods. *J. Phys. Chem. B* **2006**, *110*, 3990–3994.

54. Lutz, M. B.; Kukutsch, N.; Ogilvie, A. L. J.; Rößner, S.; Koch, F.; Romani, N.; Schuler, G. An Advanced Culture Method for Generating Large Quantities of Highly Pure Dendritic Cells from Mouse Bone Marrow. *J. Immunol. Methods* **1999**, *223*, 77–92.